Plasma formation in diode pumped alkali lasers sustained in Cs

Aram H. Markosyan[a),b)] and Mark J. Kushner[a)]

Electrical Engineering and Computer Science Department, University of Michigan, 1301 Beal Ave., Ann Arbor, Michigan 48109-2122, USA

In diode pumped alkali lasers (DPALs), lasing action occurs on the resonant lines of alkali atoms following pumping by broadband semiconductor lasers. The goal is to convert the efficient but usually poor optical quality of inexpensive diode lasers into the high optical quality of atomic vapor lasers. Resonant excitation of alkali vapor leads to plasma formation through the excitation transfer from the ^2P states to upper lying states, which then are photoionized by the pump and intracavity radiation. A first principles global model was developed to investigate the operation of the He/Cs DPAL system and the consequences of plasma formation on the efficiency of the laser. Over a range of pump powers, cell temperatures, excitation frequency, and mole fraction of the collision mixing agent (N_2 or C_2H_6), we found that sufficient plasma formation can occur that the Cs vapor is depleted. Although N_2 is not a favored collisional mixing agent due to large rates of quenching of the ^2P states, we found a range of pump parameters where laser oscillation may occur. The poor performance of N_2 buffered systems may be explained in part by plasma formation. We found that during the operation of the DPAL system with N_2 as the collisional mixing agent, plasma formation is in excess of 10^{14}–$10^{15}\,\mathrm{cm}^{-3}$, which can degrade laser output intensity by both depletion of the neutral vapor and electron collisional mixing of the laser levels. *Published by AIP Publishing.* [http://dx.doi.org/10.1063/1.4967749]

I. INTRODUCTION

Semiconductor diode lasers have the advantage of producing high power with high electrical-to-optical efficiency; however, they typically suffer from poor optical quality.[1] First demonstrated in 2003,[2] the diode pumped alkali laser (DPAL) is a method whereby the usually poor optical quality of intensity from inexpensive laser diodes can be converted into the high optical quality radiation from an atomic laser. The DPAL concept was a response to the challenges that faced diode-pumped solid state lasers[3] to achieve near-diffraction-limited operation due to thermo-optical phenomena inherent to solid state gain media such as mechanical stress-birefringence and thermally induced focusing. In a DPAL, diode lasers are used to optically pump a mixture of a rare gas and an alkali vapor, obtaining lasing action on the resonance line of the alkali vapor. The alkali vapor as an optical gain media has a relatively narrow optical bandwidth of a few tenths of a nanometer. DPAL devices therefore have the ability to efficiently convert the relatively broadband (1–3 nm) and low-brightness ($M^2 \approx 1000$) output of commercial laser diode pump arrays into high-brightness laser emission. Since DPAL pumping of the alkali laser occurs on the resonant transition of the alkali atom, the quantum energy defect ($1 - \lambda_{pump}/\lambda_{laser}$) is only 2%–4%, enabling potentially high system efficiency.[4–9]

In DPAL, the resonant transition of the alkali atom, typically the $^2P_{3/2} \rightarrow {}^2S_{1/2}$ (D$_2$ line), is pumped by the diode laser followed by collisional quenching of the alkali atom to the $^2P_{1/2}$ level. Lasing then occurs on the $^2P_{1/2} \rightarrow {}^2S_{1/2}$ transition (D$_1$ line). These conditions require that the upper laser level is inverted with respect to the ground state of the alkali atom. Recent studies of Rb and K based DPAL have yielded total efficiencies in excess of 50% (Refs. 4 and 5) and slope efficiencies in excess of 80%.[6] Models predict efficiencies exceeding 90%. Our interest here is on the DPAL using Cs vapor.

LIBORS (laser ionization based on resonance saturation), first proposed by Measures,[10] is an efficient means for producing plasmas in alkali vapor with a low intensity laser. The absorption of pump radiation by the resonant line (D$_1$ or D$_2$) of the alkali produces a large density of the $^2P_{1/2,3/2}$ states. Electron heating by super-elastic relaxation of the laser produced ^2P states can rapidly avalanche the alkali vapor by electron impact to nearly full ionization.[10] Energy pooling ($M^* + M^* \rightarrow M^{**} + M$) or electron impact excitation ($e + M^* \rightarrow M^{**} + e$) processes transfer excitation from ^2P states to upper lying states, which may then be photoionized by the pump. In many alkali vapors, the process can be initiated by associative ionization ($M^* + M^* \rightarrow M_2^+ + e$) of the resonant states. The associative ionization process in Cs is endothermic for the lowest resonant states and so requires states higher than Cs($6^2P_{1/2}$, $6^2P_{3/2}$) to directly form the dimer ion at moderate gas temperatures. With pre-existing or laser generated seed electrons, super-elastic electron heating and photoionization during DPAL operation may result in plasma formation through a LIBORS-like process. The resulting plasma may then have potential to reduce or quench laser oscillation through electron collision mixing. Huennekens *et al.*[11] experimentally investigated the ionization and population of high-lying atomic states in Cs by resonant excitation of Cs(7 P) states. They found that the resonant excitation

a)armarkos@umich.edu and mjkush@umich.edu
b)Present address: Sandia National Laboratory, 7011 East Ave., Livermore, California 94550, USA. Electronic mail: amarkos@sandia.org

resulted in formation of plasma sustained by electron impact ionization, which increases with power, where the electrons are previously heated by superelastic collisions. The potential for plasma formation during DPAL operation in Cs vapor is the focus of this paper.

Plasma formation in Cs vapor is one potential avenue for decreasing laser power. Gas heating followed by rarefaction is another factor that may detrimentally affect laser performance. Although the energy defect in DPAL is small, it is finite, and saturation of the laser levels may not be complete. The residual pump power then produces gas heating and rarefaction of the laser media. Gas heating and rarefaction have been experimentally observed and are known to produce degradation in laser performance.[12–17] Shaffer et al.[18] experimentally measured two-dimensional temperature profiles of the Cs-methane DPAL, where methane is used as a collisional relaxant to convert $^2P_{3/2}$ to $^2P_{1/2}$. They found that with a 20 W continuous pump and the DPAL operating at 9 W, the gas temperature increased by 58 °C. Vadla et al.[12] showed that resonant excitation of the 6 P states of Cs vapor also resulted in plasma formation and gas heating. They suggested that direct conversion of the energy of laser produced excited states to the kinetic energy of the atoms may be a contributing factor to gas heating and rarefaction. This mechanism requires strong pumping and a large ground state Cs density. Barmashenko et al.[19] found that ionization during Cs DPAL likely has a weak effect on the laser operation, although the power not emitted as laser intensity will be directly transferred to gas heating. The detrimental effects of gas heating in DPAL can be addressed by convective cooling from flowing gas.[19–22] Barmashenko et al.[19] developed a semi-analytical model of a DPAL using flowing gas and found that laser power can be increased during high power pumping by convective cooling.

In this paper, results from a computational investigation of the pulsed DPAL system in He/Cs mixtures are discussed. Pumping is on the $6^2S_{1/2} \rightarrow 6^2P_{3/2}$ D$_2$(852.35 nm) transition of Cs with lasing occurring on the $6^2P_{1/2} \rightarrow 6^2S_{1/2}$ D$_1$(894.59 nm) transition. The collisional mixing agent transfers excitation from $6^2P_{3/2}$ to $6^2P_{1/2}$. Two collisional transfer species were investigated. The first most common collisional relaxant use for Cs DPAL is ethane, C$_2$H$_6$. The second is nitrogen, N$_2$. Due to the high quenching coefficient by N$_2$ for the Cs(6^{2}P) states, laser oscillation is difficult to achieve with N$_2$. However, this investigation is focused on the possible formation of plasma and its consequences on laser action. The behavior between C$_2$H$_6$ and N$_2$ is distinctly different in this regard, and so a comparison of the two buffer gases provides insights into fundamental processes in plasma formation. In spite of the challenges of DPAL with an N$_2$ buffer, we have computationally found a regime where operating with a high pump rate and highly saturated laser transitions may allow laser oscillation. Although not the focus of this paper, these results may nevertheless also provide insights into a new operating regime for DPAL.

A parametric study of the plasma production and laser operation was performed as a function of the collisional relaxant and its mole fraction, pump power and cell temperature (Cs vapor pressure), and pulse shape and repetition frequency. The model consists of 43 species and many

hundreds of reactions. With such a large number of reactions, it is difficult to follow the interaction pathways of each species responsible for the generation or losses of the species of interest.[23] To provide insights into these processes, the analysis tool PumpKin was used.[23] PumpKin is a post-processing tool[24] which aids in identifying mechanisms by combining elementary reactions that produce and consume the short-lifetime (fast) species into reactive pathways.

We found that plasma formation may occur having electron densities up to 10^{14} cm^{-3} (for C$_2$H$_6$ collisional relaxant) and 10^{15} cm^{-3} (for N$_2$) for high pulse repetition frequency and high pump powers of 20–50 kW/cm^2. These plasma densities correspond to the Cs being up to 80% ionized. The plasma density builds up on a pulse-to-pulse basis and reaches a pulse-periodic steady state after 5–80 pulses (depending on power and pulse shape). The plasma formation decreases laser intensity by depletion of the Cs and by collisional quenching of the laser levels. The model used in this investigation is described in Sec. II. DPAL operation and plasma formation are discussed in Sec. III. Our concluding remarks are in Sec. IV.

II. DESCRIPTION OF THE MODEL

The model used in this investigation is Global_Kin, a global plasma kinetics model that is described in Ref. 25. In Global_Kin, rate equations for species densities, temperatures, pump intensities, and laser intensities are integrated as a function of time over successive pulsed periods. Electron impact processes are included for elastic and inelastic collisions, including electronic and vibrational excitation, superelastic collisions, ionization, and recombination. All rate coefficients for electron impact processes are functions of electron temperature, T_e, which is determined by solving an electron energy conservation equation. The rate coefficients are obtained from solutions of Boltzmann's equation for the electron energy distribution function.

The DPAL systems we investigated were sustained in mixtures of He/Cs/M, where M is either N$_2$ or C$_2$H$_6$. The energy levels of the Cs atom as well as allowed spectroscopic transitions between the excited states are shown in Fig. 1. The pumping occurs at D$_2$(852.35 nm), on the Cs(6^{2}S$_{1/2}$) $\rightarrow$ Cs(6^{2}P$_{3/2}$) transition and lasing occurs on the D$_1$(894.59 nm) transition, Cs(6^{2}P$_{1/2}$) $\rightarrow$ Cs(6^{2}S$_{1/2}$).
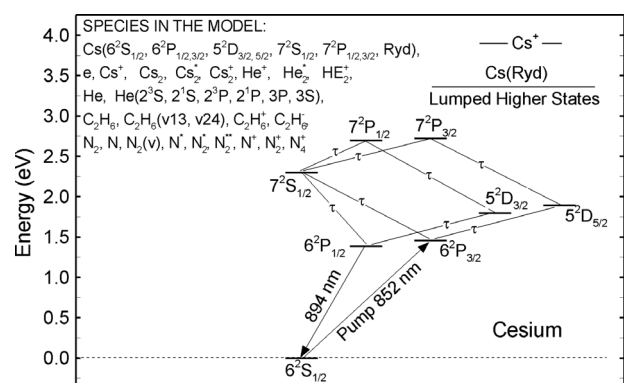

FIG. 1. Energy level diagram for cesium (Cs) DPAL and species in the mode.

Collisional mixing (spin orbit relaxation) of the $^2P_{3/2}$ and $^2P_{1/2}$ levels is the key part of this three-level (in fact, a quasi-two-level) laser scheme. During the spin-orbit relaxation, an electron in the $^2P_{3/2}$ state is transferred to $^2P_{1/2}$ state through inelastic collisions with a buffer gas. The energy difference between the ^2P levels is transferred to translational, rotational, or vibrational modes of the buffer gas or the translational energy of the Cs atom. It is critical that the buffer gas not unnecessarily quench the ^2P population to the $^2S_{1/2}$ ground level, as this will degrade laser efficiency and increase gas heating. This means that the buffer gases should have relatively large mixing rate (cross section) and small quenching rates of the ^2P levels.

The reaction mechanism includes 471 reactions for He/C_2H_6/Cs and 515 reactions for He/N_2/Cs among the following species: e, Cs($6^2S_{1/2}$, $6^2P_{1/2}$, $6^2P_{3/2}$, $5^2D_{3/2}$, $5^2D_{5/2}$, $7^2S_{1/2}$, $7^2P_{1/2}$, $7^2P_{3/2}$, Ryd), Cs^+, Cs_2, Cs_2^+, Cs_2^*, He, He_2^*, He^+, He_2^+, He(2^3S, 2^1S, 2^3P, 2^1P, 3P, 3S), N, N^+, N^*, N_4^+, N_2, $N_2(v)$, N_2^*, N_2^{**}, N_2^+, C_2H_6, C_2H_6(v13, v24), $C_2H_6^+$, $C_2H_6^+$, and $C_2H_6^-$. The diode laser pump intensity, φ_p, and laser intensities for the Cs($6^2P_{1/2}$) → Cs($6^2S_{1/2}$) transition, φ_l(894.59 nm) and the Cs($6^2P_{3/2}$) → Cs($6^2S_{1/2}$) transition, φ_2(852.35 nm), are also included. The electron impact cross sections for Cs were calculated using fully relativistic all-electron B-spline R-matrix (BSR) with pseudo-states ansatz with 311 coupled states.[26] The model includes all electron impact processes with He, C_2H_6, and Cs. Loss mechanisms for charged particles, such as diffusion and recombination on walls, are also included, although for the conditions of interest collisional radiative recombination is the dominant charged particle loss mechanism. The initial Cs/Cs_2 densities were determined by the vapor pressure based on the temperature of the cell (350 K–450 K). Gas temperature is also computed, and the consequences of rarefaction are coupled to plasma formation through changes in densities and rate coefficients in the appropriate rate equations. We used the same laser cell as described in Ref. [26], which is a 5 cm long resonator with a rear mirror having 100% reflectivity and output coupler with 98% reflectivity for the laser wavelength. We assume that the laser is longitudinally pumped with single pass of the pump beam.

As discussed below, plasma formation results from excitation transfer of Cs(6^2P) states produced by the pump to higher lying excited states. The higher lying states enable Penning reactions [e.g., Cs($6^2P_{1/2}$) + Cs($7^2P_{1/2,3/2}$,Ryd) → Cs^+ + Cs + e] or photoionization by the pump laser to produce plasma. The plasma is then self-sustained by superelastic heating from all of the Cs excited states [e + Cs* → Cs + e_{hot}]. Depending on operating conditions (e.g., cell temperature, pump intensity, collisional relaxant agent), the excitation transfer out of the Cs(6^2P) results from electron impact or by energy pooling reactions [Cs(6^2P) + Cs(6^2P) → Cs + Cs**].

III. DPAL OPERATION AND PLASMA FORMATION

Pumping of DPAL is typically characterized by low power and long pulse length, or cw pumping. In order to examine high pumping rates that may provide laser oscillation with an N_2 buffer, pulsed excitation was examined. As a

base case, the diode laser pump at 852 nm had a 1 μs pulse length with 50 ns rise and fall times, with a pulse repetition frequency (PRF) of 1 kHz. At least 100 pump cycles were simulated to achieve a pulse-periodic steady state in laser intensities and excited state densities. The pump cell was maintained at 400 K while containing 600 Torr of He and Cs vapor ([Cs] = 7.1×10^{13} cm^{-3}, mole fraction 4.9×10^{-6}). When adding the collisional relaxant (N_2 or C_2H_6), the mole fraction of He was adjusted to maintain the total pressure at 600 Torr for the initial temperature. The collisional relaxant mole fraction was varied from 0.001 to 0.5. The pump intensities were varied from 0.5 to 50 kW/cm^2, pump pulse repetition frequencies from 1 to 25 kHz, and the cell temperatures were varied from 350 to 450 K. By keeping pump energy per pulse (10 kW/cm^2 × 1 μs) and repetition frequency (1 kHz) constant, we varied the pulse length from 0.1 to 5 μs. The pulse-periodic steady state results were not sensitive to the value of initial electron density, which was 10^6 cm^{-3}.

The density of species responsible for lasing are shown in Fig. 2 for the 100th pulse for a 20 kW/cm^2 pump for the He/M/Cs = 85/15/4.9×10^{-6} (M = N_2 or C_2H_6) DPAL system. The laser is operating. For the N_2 buffer, a pulse-
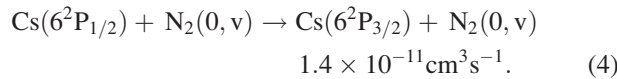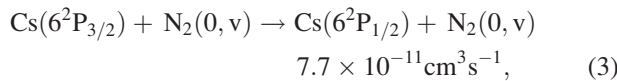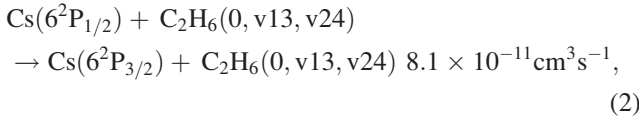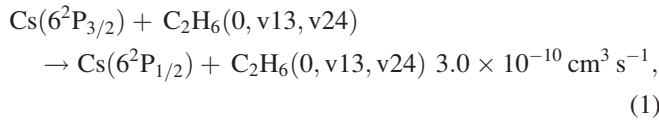

(a)

(b)
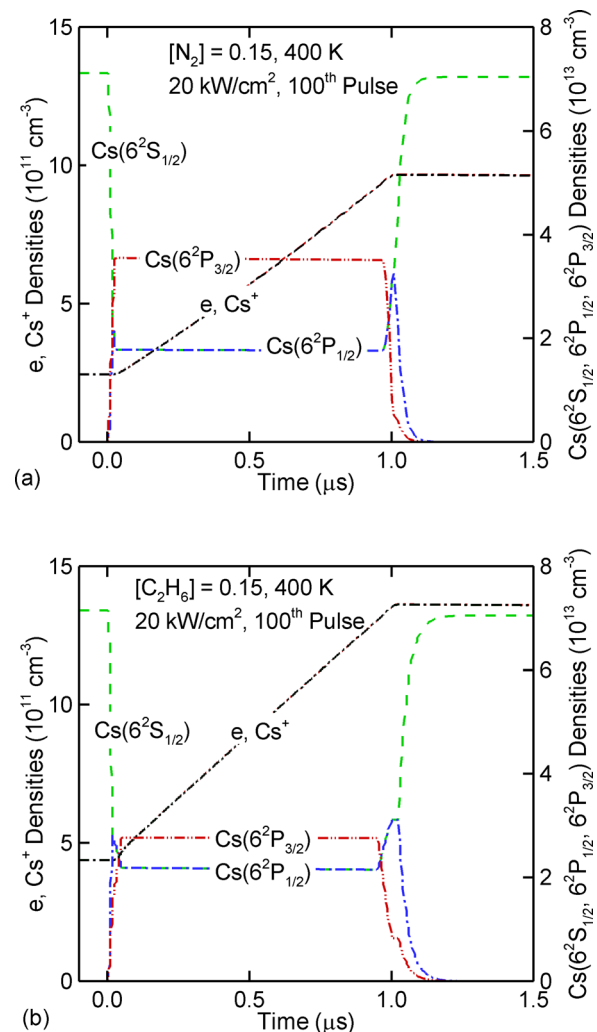
FIG. 2. Density of species responsible for lasing at 894 nm during the 100th pulse for buffer mole fractions of (a) [N_2] = 0.15 and (b) [C_2H_6] = 0.15. The total pressure is 600 Torr.

periodic steady state is reached after only 5 pump pulses. At the beginning of the pump pulse, the electron density is 2.5×10^{11} cm^{-3}, rising to 9×10^{11} cm^{-3} during the pump pulse. During the inter-pulse period, collisional radiative recombination ($Cs^+ + e + e \rightarrow Cs(6^2P_{1/2,3/2}) + e$) reduces the electron density to the pre-pulse value. In C_2H_6, this range of electron density is $(4.5–14) \times 10^{11}$ cm^{-3}. The ion density consists essentially of Cs^+. Upon starting of pumping (t = 0 in the figures), the $Cs(6^2S_{1/2})$ ground state is depleted by the pump with approximately half of its population appearing in each of the $Cs(6^2P_{1/2,3/2})$. With laser oscillation on the $Cs(6^2P_{1/2}) \rightarrow Cs(6^2S_{1/2})$ D$_1$(894.59 nm) transition, the ratio of the degeneracies of the upper and lower laser levels is the same. Upon reaching threshold, laser oscillation heavily saturates the laser transitions and the densities of these two states are essentially the same. The density of the $Cs(6^2P_{3/2})$, which is being pumped, is higher than that of the saturated laser levels.

The pump pulse depletes the population of the ground state $Cs(6^2S_{1/2})$ into the $Cs(6^2P_{1/2})$ and $Cs(6^2P_{3/2})$ excited states. The buffer gas (ethane or nitrogen) then collisionally relaxes the $Cs(6^2P_{3/2})$ to the $Cs(6^2P_{1/2})$, which upon stimulated emission on the D$_1$(894.59 nm) transition line and repopulates the ground state $Cs(6^2S_{1/2})$. The rate coefficient for collisional relaxation of the $^2P_{3/2}$ state to the $^2P_{1/2}$ state by N_2 is 7.7×10^{-11} cm^3 s^{-1} (Ref. 27) and by C_2H_6 is 3.0×10^{-10} cm^3 s^{-1} at 300 K.[27,28]

$$Cs(6^2P_{3/2}) + C_2H_6(0, v13, v24)$$
$$\rightarrow Cs(6^2P_{1/2}) + C_2H_6(0, v13, v24) \ 3.0 \times 10^{-10} \ cm^3 \ s^{-1},$$
(1)

$$Cs(6^2P_{1/2}) + C_2H_6(0, v13, v24)$$
$$\rightarrow Cs(6^2P_{3/2}) + C_2H_6(0, v13, v24) \ 8.1 \times 10^{-11} cm^3 s^{-1},$$
(2)

$$Cs(6^2P_{3/2}) + N_2(0, v) \rightarrow Cs(6^2P_{1/2}) + N_2(0, v)$$
$$7.7 \times 10^{-11} cm^3 s^{-1},$$
(3)

$$Cs(6^2P_{1/2}) + N_2(0, v) \rightarrow Cs(6^2P_{3/2}) + N_2(0, v)$$
$$1.4 \times 10^{-11} cm^3 s^{-1}.$$
(4)

For otherwise the same pump conditions, the lower rate of quenching of $^2P_{3/2}$ to $^2P_{1/2}$ by N_2 results in the density of $^2P_{3/2}$ being higher (3.5×10^{13} cm^{-3}) with N_2 as a buffer than C_2H_6 (2.7×10^{13} cm^{-3}). The larger density of $^2P_{3/2}$ then results in a lower saturation density of the $^2P_{1/2}$ and $^2S_{1/2}$ during oscillation with N_2, 1.7×10^{13} cm^{-3}, compared with 2.1×10^{13} cm^{-3} with C_2H_6 as the buffer. The lower saturated densities result in lower laser intensity. On the other hand, higher $^2P_{3/2}$ densities result in higher electron heating by superelastic relaxation.

The electron and gas temperatures, shown in Fig. 3, rise on a pulse-to-pulse basis and reach pulse periodic steady state values after tens of pulses. The electron temperature, T_e, increases during the pump pulse from essentially being in thermal equilibrium with the gas (0.03 eV or 400 K) to 0.2 eV in N_2. The modulation of T_e during pumping with C_2H_6 is
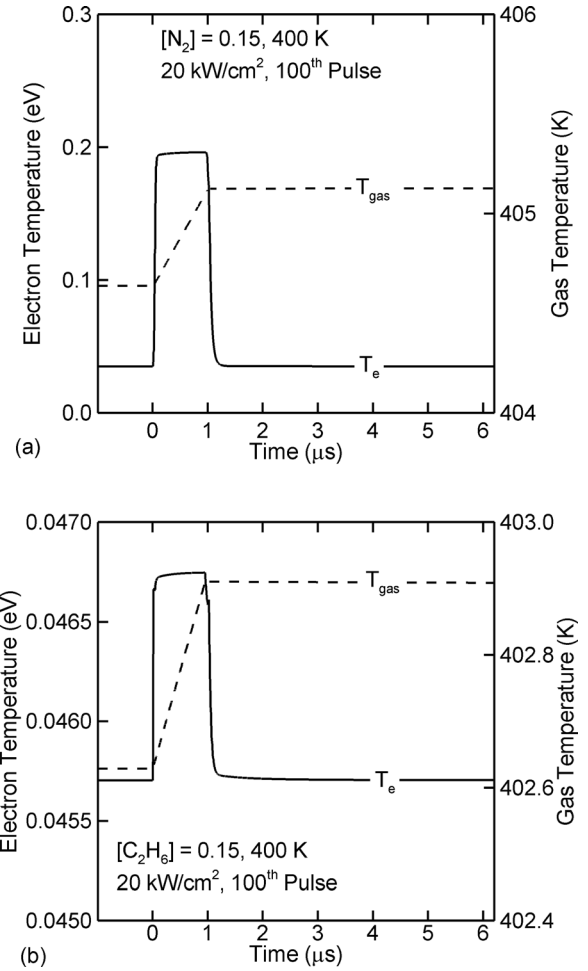

FIG. 3. Electron and gas temperatures when lasing at 894 nm during the 100th pulse for buffer mole fractions of (a) [N_2] = 0.15 and (b) [C_2H_6] = 0.15.

small. The heating of electrons is dominant by superelastic relaxation of the $Cs(^2P)$ states.[26] Since the rate of excitation of $Cs(^2P)$ is essentially the same in both systems, the rate of electron heating is also essentially the same. The electron energy is dissipated by electron impact excitation of the $Cs(^2P)$ states to higher levels, and by electron impact excitation of the vibrational states of the collisional mixer. The cross sections for vibrational excitation of N_2 have a higher threshold (1.3 eV) compared with the threshold energy for C_2H_6 (0.15 eV), and so the rate coefficients for electron impact vibrational excitation of C_2H_6 are significantly larger than for N_2 at low electron temperatures. Therefore, the power acquired by electrons through superelastic relaxation of $Cs(^2P)$ is rapidly dissipated by vibrational excitation of C_2H_6, which then produces a lower T_e.

Energy pooling collisions between $Cs(6^2P_{1/2})$ atoms populate the $Cs(7^2P_{1/2,3/2})$ states with a rate coefficient of 7.0×10^{-10} cm^3 s^{-1} and the high-lying Rydberg levels $Cs^* + Cs^* \rightarrow Cs \ Cs(Ryd)$ with a rate coefficient of 1.0×10^{-10} cm^3 s^{-1}.[29] Once these Cs upper states are formed, excitation transfer back to the buffer can populate vibrational states of nitrogen and ethane: $N_2 + Cs^* \rightarrow N_2(v) + Cs$ with a rate coefficient of 6.3×10^{-12} cm^3 s^{-1} and $C_2H_6 + Cs^* \leftrightarrow C_2H_6(v13, v24) + Cs$ with a rate coefficient of

$3.3 \times 10^{-12} \, \text{cm}^3 \, \text{s}^{-1}$.[30] Vibrational-translational (V-T) relaxation leads to the thermalization of the vibrational energy of the molecules, a process that is faster with C_2H_6.[30]

Penning and associative ionization by Cs excited states higher than 7 P are exothermic, with the excess energy carried by the emitted electron with energies from 0.01 eV to 1.71 eV. These associative and Penning ionization reactions, as well as the superelastic collisions, can transfer energy from excited atoms into the electrons. The electron impact cross sections for excitation of Cs, similar to other alkali atoms, are large with values of greater than $100 \, \text{Å}^2$ at energies of a few eV.[26] These large cross sections enable the efficient coupling of the electrons to the excited states of Cs and are in part responsible for efficient laser-induced plasma formation in alkali vapors.[12,26]

The electron density and laser output intensity of the 894 nm transition as a function of the mole fraction of N_2 and C_2H_6 are shown in Fig. 4. In spite of the rapid quenching of Cs(6 P) by N_2, at sufficiently high pump rates, laser oscillation occurs. Three regions of operation occur for both of the gas mixtures: low mole fraction (no lasing, low electron densities), medium mole fraction (increasing lasing intensity, increasing electron density), and high mole fraction
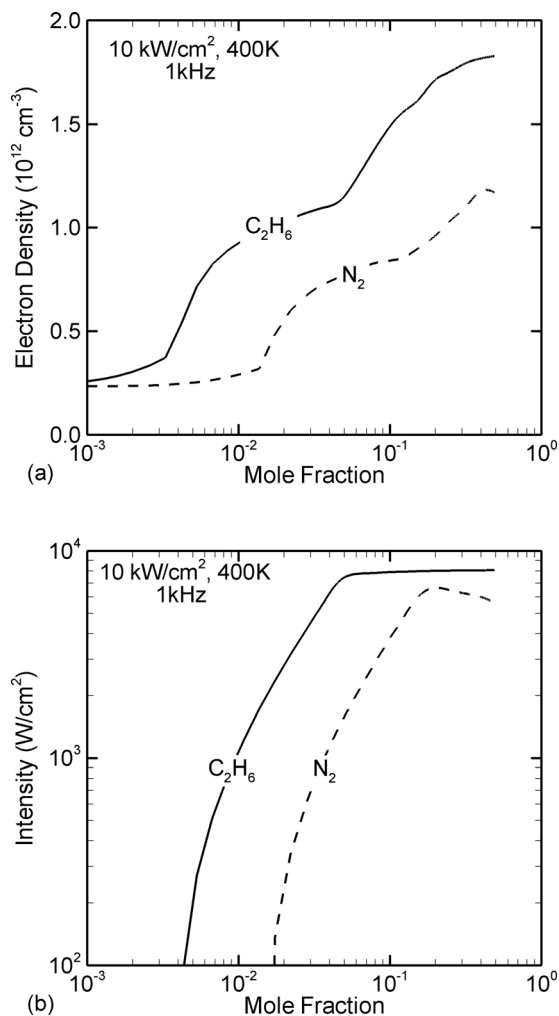

FIG. 4. System performance as a function of the mole fraction of C_2H_6 and N_2. (a) Electron densities and (b) laser intensity at 894 nm.

(saturated lasing intensity, increasing electron density). In the first regime, a low mole fraction of buffer gas results in insufficient collisional relaxation of Cs($6^2P_{3/2}$) to Cs($6^2P_{1/2}$), which produces low electron densities and no lasing. In the next regime, the increase in quencher mole fraction results in an increase in lasing intensities up to their saturated values while the electron density continues to increase. The thresholds of this regime are mole fractions of 0.003 for ethane and 0.01 for nitrogen. In the next regime, the laser intensities are saturated due to the finite pump power. The thresholds of this regime are 0.05 for ethane and 0.2 for nitrogen, with the differences being due to the higher rates of collisional mixing by ethane.

IV. PUMP-PULSE LENGTH AND FREQUENCY

An important factor affecting the laser performance is the length of the pump pulse. The laser intensity and electron density are shown in Fig. 5 for pump pulse lengths of 0.1–5 μs while keeping the frequency (1 kHz), cell temperature (400 K), and pump energy per pulse constant (10 kW/cm^2 × 1 μs = 10 mJ/cm^2). When increasing the pulse length while keeping the energy per pulse constant, the pump intensity decreases. So higher pump intensities in the figure correspond to shorter pulse lengths. As a reference, in Fig. 5 we also show the laser intensity and the electron density for a constant 1 μs pulse while varying pump intensity. For a constant pulse length, increasing pump laser intensity increases pump energy. For pump intensities below 10 kW/cm^2 (or pulse lengths of 1–5 μs), the laser intensity is determined by the input power and it is not sensitive to changes in pulse length or total pump energy. For pump powers up to 3.5 kW/cm^2, the electron density increases. On the other hand, the electron density is sensitive to pulse length. In spite of the pump intensity being lower, the longer pulse lengths enable the electron density to continue to build to higher values. With high pump intensities, the shorter pulse length results in a lower electron density.

Pump-pulse frequency provides additional control on plasma formation and can significantly affect the laser performance. The electron density and laser intensity for the 894 nm transition as a function of pump repetition frequencies of 1–25 kHz for N_2 containing mixtures are shown in Fig. 6. With a fixed 1 μs pulse length increasing, pulse repetition frequency decreases the inter-pulse period. The shorter inter-pulse period allows the electron density to accumulate on a pulse-to-pulse basis, thereby producing higher average electron densities. The higher electron densities excite the Cs(^{2}P) to higher levels. These Cs* densities then deplete the laser levels in associative and Penning ionization reactions, or by energy-pooling reactions. As a result, the Cs($6^2P_{1/2}$) densities and hence the laser intensities decrease with increasing pulse repetition frequency.

V. PUMP INTENSITY AND TEMPERATURE

Peak laser intensities at 894 nm for Cs cell temperatures of 350–450 K (1 kHz, 1 μs pulse duration) are shown in Fig. 7 as a function of pump-pulse power. For both ethane and nitrogen buffer gases, the laser intensity increases with pump power while the threshold pump intensity increases
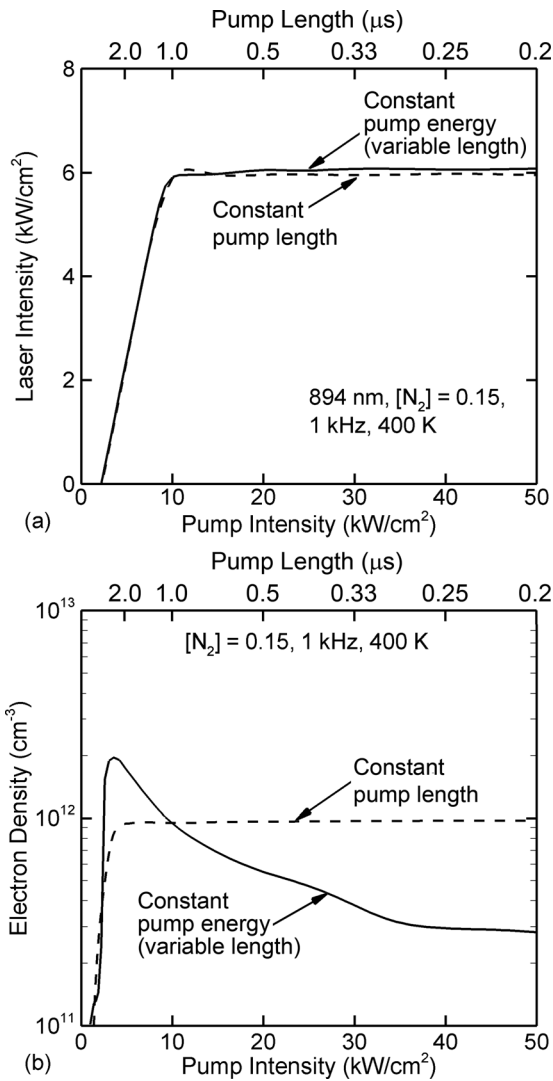
FIG. 5. System properties as a function of pump intensity for a pump frequency of 1 kHz. Results are shown for a constant pulse energy while varying pulse length (normalized to $10 \, kW/cm^2 \times 1 \, \mu s$) and for a constant pulse length (1 μs) while varying intensity. When increasing pulse intensity with constant energy per pulse, the pulse length decreases. (a) Laser intensity and (b) electron density. The temperature is 400 K and buffer mole fraction is $[N_2] = 0.15$.
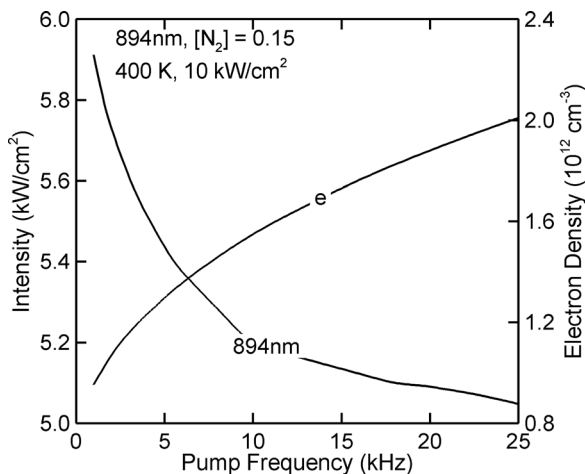

FIG. 6. Electron density and laser intensity at 894 nm as a function of pump frequency.

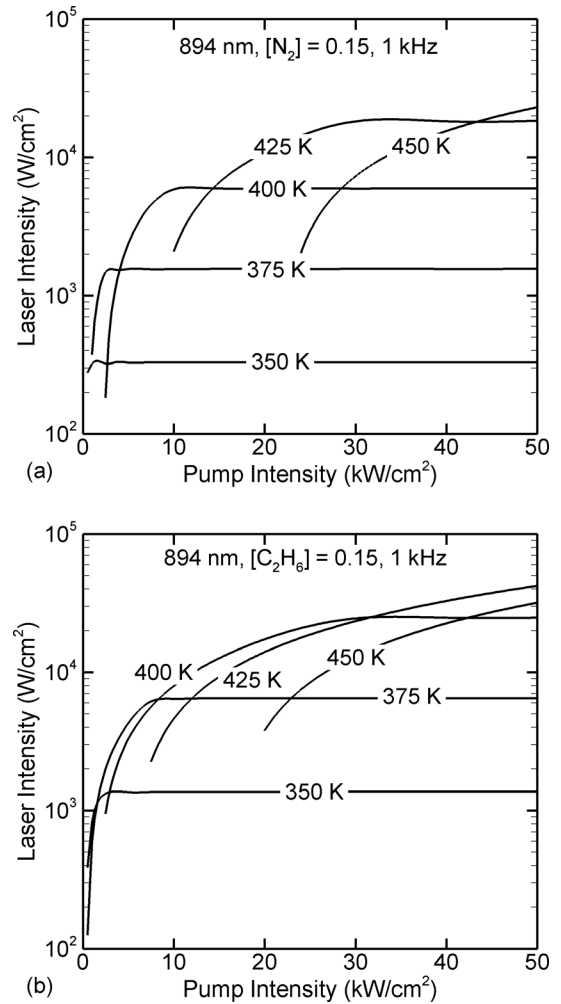FIG. 7. Laser intensity at 894 nm as a function of the pump intensity for buffers of (a) N_2 and (b) C_2H_6 for Cs cell temperatures of 350–450 K.

with cell temperature. With increasing cell temperature, the vapor pressure of Cs increases, and so an increase in pump power is needed to invert the ground state. In all cases, laser intensities eventually saturate with pump power. The saturation results from the pump rate being limited by the Cs vapor density and indicates that the maximum inversion density has been reached. The higher the temperature, the higher the Cs vapor density and, hence, the higher the possible inversion density. The 894 nm lasing efficiencies as a function of the pump intensity with nitrogen and with ethane buffers are shown in Fig. 8. DPAL with ethane as a collisional relaxant has a predicted efficiency of 80%, whereas the maximum efficiency for nitrogen relaxant is near 60%. The predicted efficiency with ethane is comparable to that measured experimentally[6] but less than the quantum efficiency of 95%. The processes limiting efficiency are energy pooling of the $Cs(6^2P)$ levels, electron excitation out of the $Cs(6^2P)$ levels to higher levels, and losses due to photoionization. These processes are discussed below. The pump power required for peak efficiency is an increasing function of cell temperature, as the higher Cs vapor pressure is able to utilize the increasing pump intensity.

Electron densities are shown in Fig. 9 as a function of pump rates and Cs cell temperatures of 350–450 K. For cell
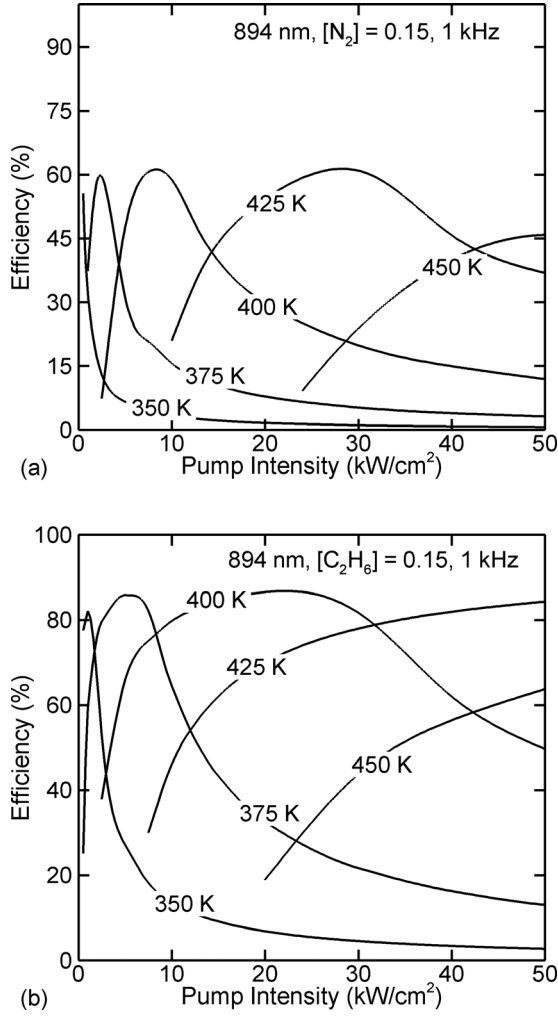
FIG. 8. Efficiency for lasing at 894 nm as a function of the pump intensity for buffers of (a) N_2 and (b) C_2H_6 for Cs cell temperatures of 350–450 K.

FIG. 9. Electron density as a function of the pump intensity for buffers of (a) N_2 and (b) C_2H_6.

temperatures less than 400 K, comparable electron densities are produced with both buffer gases. Above 400 K (and Cs vapor densities above 7.14×10^{13} cm^{-3}), the electron density for the N_2 buffer grows to be an order of magnitude higher than for C_2H_6. This increase in electron density is in large part a result of the higher electron temperature in N_2. For temperatures above 400 K, the laser intensity with the C_2H_6 buffer continues to increase with increasing pump intensity. With the N_2 buffer, laser intensities decrease at the higher pump intensities. This disparity between N_2 and C_2H_6 buffers can be attributed to the larger plasma density in N_2 which depletes the laser levels, either by ionization or excitation to higher levels.

With both buffer gases, the electron density has a significant increase between 400 K and 425 K (Cs vapor densities of 7.14×10^{13} to 2.45×10^{14} cm^{-3}). In the following analysis, we investigate the dominant pathways for the formation of plasma for an N_2 buffered system pumped at 20 kW/cm^2, where the fractional ionization [e]/[Cs] increases from 0.01 (for 400 K) to 0.38 (for 425 K). This increase in plasma density is enabled by an increase in electron temperature during the pump pulse from 0.19 eV (400 K) to 0.32 eV (450 K).

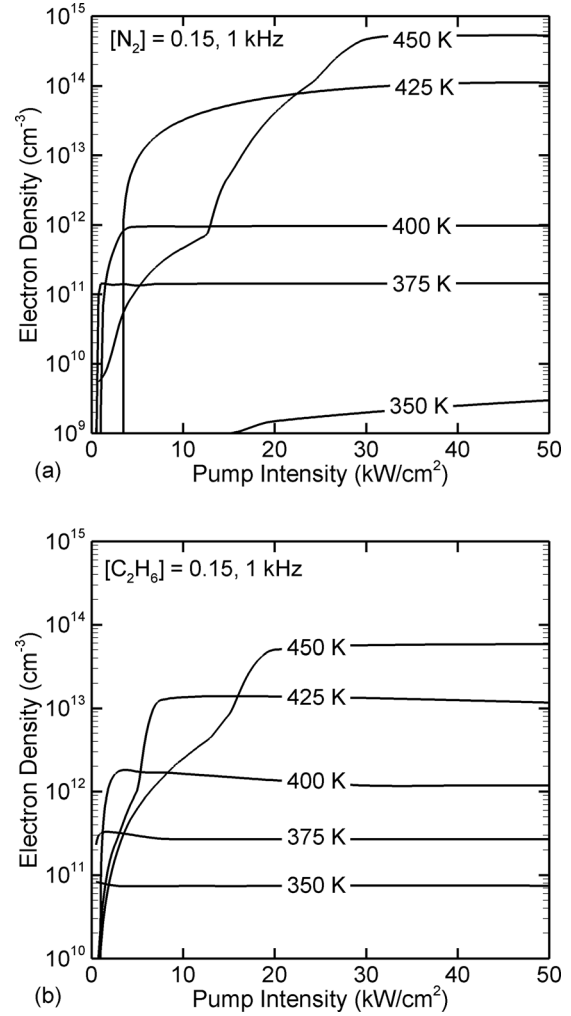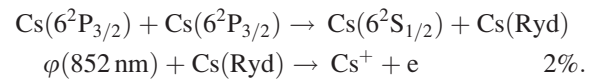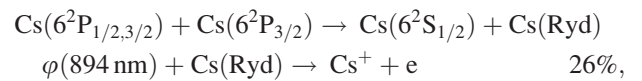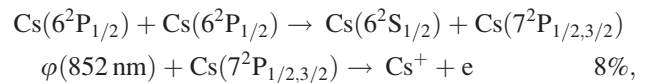400 K: The pump excites Cs($6^2S_{1/2}$) into the Cs($6^2P_{3/2}$) state, and the collisional relaxant (N_2 in this case) transfers excitation from Cs($6^2P_{3/2}$) to Cs($6^2P_{1/2}$). The dominant plasma forming pathways are then

$$Cs(6^2P_{1/2}) + Cs(6^2P_{1/2}) \rightarrow Cs(6^2S_{1/2}) + Cs(7^2P_{1/2,3/2})$$
$$\varphi(894 \text{ nm}) + Cs(7^2P_{1/2,3/2}) \rightarrow Cs^+ + e \qquad 63\%,$$

$$Cs(6^2P_{1/2}) + Cs(6^2P_{1/2}) \rightarrow Cs(6^2S_{1/2}) + Cs(7^2P_{1/2,3/2})$$
$$\varphi(852 \text{ nm}) + Cs(7^2P_{1/2,3/2}) \rightarrow Cs^+ + e \qquad 8\%,$$

$$Cs(6^2P_{1/2,3/2}) + Cs(6^2P_{3/2}) \rightarrow Cs(6^2S_{1/2}) + Cs(Ryd)$$
$$\varphi(894 \text{ nm}) + Cs(Ryd) \rightarrow Cs^+ + e \qquad 26\%,$$

$$Cs(6^2P_{3/2}) + Cs(6^2P_{3/2}) \rightarrow Cs(6^2S_{1/2}) + Cs(Ryd)$$
$$\varphi(852 \text{ nm}) + Cs(Ryd) \rightarrow Cs^+ + e \qquad 2\%.$$
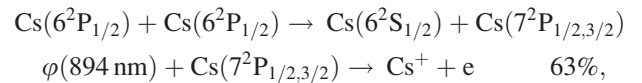
The excitation pooling reactions between two Cs(6^2P) states populate the higher Cs(7^2P) and Rydberg states, which later are photoionized primarily by 894 nm photons. This mechanism explains 97% of plasma formation.

Another important species contributing to the plasma formation, and electron and gas heating, are Cs($5^2D_{3/2,5/2}$) and Cs($7^2S_{1/2}$) states. The Cs($5^2D_{3/2,5/2}$) states are dominantly formed by electron impact of the Cs(6^2P). They are quenched

dominantly by collisions with N_2 (90%), which contributes to gas heating, and radiative relaxation (10%). The formation of $Cs(7^2S_{1/2})$ is dominantly by electron impact of $Cs(6^2P)$. The $Cs(7^2S_{1/2})$ is then photoionized (56%) and quenched by collisions with N_2 (33%) which contributes both to increasing the electron density and gas heating.

425 K: When the Cs cell temperature is increased, the pathways responsible for the plasma formation change dominantly to photoionization of $Cs(7^2S_{1/2})$.

$$e + Cs(6^2P_{3/2}) \rightarrow Cs(7^2S_{1/2}) + e$$
$$\varphi(894\,nm) + Cs(7^2S_{1/2}) \rightarrow Cs^+ + e \quad 76\%,$$
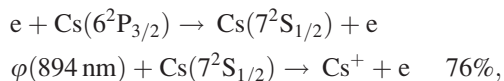
while the remaining plasma is formed by the photoionization of $Cs(7^2P)$ and Rydberg states by 894 nm (16%) and 852 nm (8%) photons. The production of $Cs(5^2D_{3/2,5/2})$ and $Cs(7^2S_{1/2})$ is similar to that at 400 K, but the destruction mechanisms differ. At the higher temperature and larger Cs density, about 40% of the $Cs(5^2D_{3/2})$ and 44% of the $Cs(7^2S_{1/2})$ are quenched by superelastic electron collisions to $Cs(6^2P_{1/2,\,3/2})$. These superelastic collisions heat the electrons and are responsible for the higher electron temperature of 0.32 eV at 425 K compared with 0.19 eV at 400 K. The higher electron temperature is then responsible for the production of $Cs(7^2S)$ by direct electron impact on $Cs(6^2P)$. The higher densities of $Cs(7^2S)$ then enable photoionization, which eventually depletes the neutral Cs.

In summary, when operating at a cell temperature of 400 K (Cs density $7.14 \times 10^{13}\,cm^{-3}$) the plasma formation is largely explained by the energy pooling reactions of $Cs(6^2P)$, which populates higher excited states of Cs. At the higher Cs densities ($2.45 \times 10^{14}\,cm^{-3}$) at 425 K and above, these higher excited states are produced by electron impact excitation of the $Cs(6^2P)$, which is facilitated by superelastic electron heating.

VI. CONCLUDING REMARKS

A computational parametric study of the kinetics of the Cs pulsed DPAL was performed for ethane and nitrogen collisional relaxants. A pulse-periodic steady state was reached after tens of pulses. The choice of relaxing agent affects plasma formation and, consequently, laser performance. At low system temperatures and low Cs vapor densities, plasma is formed with densities $10^{12}\,cm^{-3}$ with both buffers produced largely by photoionization by the pump and laser. The higher lying states that are photoionized are produced by energy pooling reactions. These densities of both higher lying states and of Cs^+ do not significantly affect laser performance. With increasing temperature and increasing Cs vapor density, the lower collisional mixing of the $Cs(6^2P)$ levels by N_2 enables higher electron temperatures compared with the C_2H_6 buffer. These higher electron temperatures are supported by superelastic collisions and produce the higher lying states which are then photoionized producing higher plasma densities to $10^{15}\,cm^{-3}$. The higher plasma densities ultimately limit laser performance through depletion of Cs vapor by formation of Cs^+ and collisional mixing of the laser levels.

Benchmark experiments to determine the influence of plasma formation on laser performance may be difficult to perform as, for example, the use of electrical probes is challenging at high pressures. A possible benchmark experiment is adding a small amount of a highly attaching gas that would not perturb the laser kinetics but would consume low energy electrons.

Ionization of both N_2 and C_2H_6 are included in the reaction mechanism, as is electron impact dissociation of N_2. Negligible densities of either N_2^+ and $C_2H_6^+$, or of N atoms are produced due to the low electron temperatures. With the threshold for electron impact dissociation of C_2H_6 being 7.6 eV, we do not expect that there will be a significant dissociation of ethane, and so fragments of C_2H_6 were not tracked in the model. Having said that, Zhdanov and Knize observed the contamination of windows in their Cs DPAL cell, which they attributed to the reactions of the alkali atoms with ethane.[31] Plasma production of vibrationally excited C_2H_6 or even small densities of C_xH_y fragments would likely accelerate the reactions of the type observed by Zhdanov and Knize and contribute to contamination of optics.

[1]W. F. Krupke, "Diode pumped alkali lasers (DPALs): An overview," Proc. SPIE **7005**, 700521 (2008).

[2]W. F. Krupke, R. J. Beach, V. K. Kanz, and S. A. Payne, "Resonance transition 795-nm rubidium laser," Opt. Lett. **28**(23), 2336–2338 (2003).

[3]T. Y. Fan and R. L. Byer, "Diode laser pumped solid state lasers," IEEE J. Quantum Electron. **24**(6), 895–912 (1988).

[4]W. F. Krupke, J. B. Raymond, K. K. Vernon, A. P. Stephen, and T. E. James, "New class of cw high-power diode-pumped alkali lasers (DPALs)," Proc. SPIE **5448**, 7 (2004).

[5]B. V. Zhdanov, T. Ehrenreich, and R. J. Knize, "Highly efficient optically pumped cesium vapor laser," Opt. Commun. **260**, 696 (2006).

[6]B. V. Zhdanov and R. J. Knize, "Alkali lasers development at laser and optics research center of the U.S. Air Force Academy," Proc. SPIE **7005**, 700524 (2008).

[7]B. D. Barmashenko and S. Rosenwaks, "Detailed analysis of kinetic and fluid dynamic processes in diode pumped alkali lasers," J. Opt. Soc. Am. B **30**, 1118 (2013).

[8]G. Perram, "Intensity scaling for diode pumped alkali lasers," SPIE Newsroom (2012).

[9]B. V. Zhdanov, M. D. Rorondaro, M. K. Shaffer, and R. J. Knize, "Efficient potassium diode pumped alkali laser operating in pulsed mode," Opt. Express **22**, 17266 (2014).

[10]R. M. Measures, "Electron density and temperature elevation of a potassium seeded plasma by laser resonance pumping," J. Quant. Spectrosc. Radiat. Transfer **10**, 107 (1970).

[11]J. Huennekens, Z. Wu, and T. G. Walker, "Ionization, excitation of high-lying atomic states, and molecular fluorescence in Cs vapor excited at $\lambda = 455.7$ and 459.4 nm," Phys. Rev. A **31**, 196 (1985).

[12]C. Vadla, V. Horvatic, D. Veza, and K. Kiemax, "Resonantly laser induced plasmas in gases: The role of energy pooling and exothermic collisions in plasma breakdown and heating," Spectrochim. Acta B **65**, 33–45 (2010).

[13]Q. Zhu, B. Pan, L. Chen, Y. Wang, and X. Zhang, "Analysis of temperature distributions in diode-pumped alkali vapor lasers," Opt. Commun. **283**(11), 2406 (2010).

[14]R. J. Beach, W. F. Krupke, V. K. Kan, and S. A. Payne, "End-pumped continuous-wave alkali vapor lasers: Experiment, model, and power scaling," J. Opt. Soc. Am. B **21**, 2151 (2004).

[15]B. V. Zhdanov, A. Stooke, G. Boyadjian, A. Voci, and R. J. Knize, "Optically pumped cesium-Freon laser," Opt. Express **16**, 748 (2008).

[16]Ty. A. Perschbacher, D. A. Hostutler, and T. M. Shay, "High-efficiency diode-pumped rubidium laser: Experimental results," Proc. SPIE **6346**, 634607 (2007).

[17]B. V. Zhdanov, A. Stooke, G. Boyadjian, A. Voci, and R. J. Knize, "Rubidium vapor laser pumped by two laser diode arrays," Opt. Lett. **33**, 414 (2008).

[18]M. K. Shaffer, T. C. Lilly, B. V. Zhdanov, and R. J. Knize, "*In situ* non-perturbative temperature measurement in a Cs alkali laser," Opt. Lett. **40**, 1 (2015).

[19]B. D. Barmashenko, S. Rosenwaks, and M. C. Heaven, "Static diode pumped alkali lasers: Model calculations of the effects of heating, ionization, high electronic excitation and chemical reactions," Opt. Commun. **292**, 123 (2013).

[20]B. D. Barmashenko and S. Rosenwaks, "Modeling of flowing gas diode pumped alkali lasers: Dependence of the operation on the gas velocity and on the nature of the buffer gas," Opt. Lett. **37**(17), 3615 (2012).

[21]B. V. Zhdanov, J. Sell, and R. J. Knize, "Multiple laser diode array pumped Cs laser with 48 W output power," Electron. Lett. **44**, 582 (2008).

[22]A. V. Bogachev, S. G. Garanin, A. M. Dudov, V. A. Eroshenko, S. M. Kulikov, G. T. Mikaelian, V. A. Panarin, V. O. Pautov, A. V. Rus, and S. A. Sukharev, "Diode-pumped caesium vapour laser with closed-cycle laser-active medium circulation," Quantum Electron. **42**, 95 (2012).

[23]A. H. Markosyan, A. Luque, F. Gordillo-Vazquez, and U. Ebert, "PumpKin: A tool to find principal pathways in plasma chemical models," Comput. Phys. Commun. **185**, 2697–2702 (2014).

[24]A. H. Markosyan, A. Luque, F. Gordillo-Vazquez, and U. Ebert, "PumpKin: A tool to find principal pathways in plasma chemical models," 2013, see www.pumpkin-tool.org.

[25]D. S. Stafford and M. J. Kushner, "$O_2(^1\Delta)$ Production in He/O_2 mixtures in flowing low pressure plasmas," J. Appl. Phys. **96**, 2451 (2004).

[26]O. Zatsarinny, K. Bartschat, N. Yu. Babaeva, and M. J. Kushner, "Electron collisions with cesium atoms—benchmark calculations and application to modeling an excimer-pumped alkali laser," Plasma Sources Sci. Technol. **23**, 035011 (2014).

[27]G. A. Pitz, C. D. Fox, and G. P. Perram, "Transfer between the cesium $6^2P_{1/2}$ and $6^2P_{3/2}$ levels induced by collisions with H_2, HD, D_2, CH_4, C_2H_6, CF_4 and C_2F_6," Phys Rev. A **84**, 032708 (2011).

[28]A. D. Palla, D. L. Carroll, J. T. Verdeyen, and M. C. Heaven, "XPAL modeling and theory," Proc. SPIE **7915**, 79150B (2011).

[29]S. Milosevic, F. de Tomasi, F. Fuso, and M. Allegrini, "Thermal-energy pooling collisions in cesium vapour: $Cs(6P_{3/2}) + Cs(6P_{3/2}) \rightarrow Cs(7P_{3/2,\ 1/2}) + Cs(6S_{1/2})$," Europhys. Lett. **32**(9), 703–708 (1995).

[30]A. Starikovskiy and N. Aleksandrov, "Plasma-assisted ignition and combustion," Prog. Energy Combust. Sci. **39**, 61–110 (2013).

[31]B. Zhdanov and R. Knize, "Diode-pumped 10 W continuous wave cesium laser," Opt. Lett. **32**, 2167–2169 (2007).